Hydrol. Earth Syst. Sci. Discuss., 11, 13711–13744, 2014
www.hydrol-earth-syst-sci-discuss.net/11/13711/2014/
doi:10.5194/hessd-11-13711-2014

Hydrology and Earth System Sciences
Open Access
Discussions

Dye tracing for investigating flow and transport properties of hydrocarbon-polluted Rabots glaciär, Kebnekaise, Sweden

C. C. Clason[1], C. Coch[1], J. Jarsjö[1], K. Brugger[2], P. Jansson[1], and G. Rosqvist[1]

[1]Department of Physical Geography and Quaternary Geology, Stockholm University, 106 91 Stockholm, Sweden
[2]Geology Discipline, University of Minnesota-Morris, Morris, MN, 56267, USA

Received: 5 November 2014 – Accepted: 1 December 2014 – Published: 15 December 2014

Correspondence to: C. C. Clason (caroline.clason@natgeo.su.se)

Published by Copernicus Publications on behalf of the European Geosciences Union.

Abstract

Over 11 000 L of hydrocarbon pollution was deposited on the surface of Rabots glaciär on the Kebnekaise Massif, northern Sweden, following the crash of a Royal Norwegian Air Force aircraft in March 2012. An environmental monitoring programme was subsequently commissioned, including water, snow and ice sampling. The scientific programme further included a series of dye tracing experiments during the 2013 melt season, conducted to investigate flow pathways for pollutants through the glacier hydrological system, and to gain new insight to the internal hydrological system of Rabots glaciär. Results of dye tracing reveal a degree of homogeneity in the topology of the drainage system throughout July and August, with an increase in efficiency as the season progresses, as reflected by decreasing temporary storage and dispersivity. Early onset of melting likely led to formation of an efficient, discrete drainage system early in the melt season, subject to decreasing sinuosity and braiding as the season progressed. Analysis of turbidity-discharge hysteresis further supports the formation of discrete, efficient drainage, with clockwise diurnal hysteresis suggesting easy mobilisation of readily-available sediments in channels. Dye injection immediately downstream of the pollution source zone revealed prolonged storage of dye followed by fast, efficient release. Twinned with a low dye recovery, and supported by sporadic detection of hydrocarbons in the proglacial river, we suggest that meltwater, and thus pollutants in solution, may be released periodically from this zone of the glacier hydrological system. The here identified dynamics of dye storage, dispersion and breakthrough indicate that the ultimate fate and permanence of pollutants in the glacier system is likely to be governed by storage of pollutants in the firn layer and ice mass, or within the internal hydrological system, where it may refreeze. This shows that future studies on the fate of hydrocarbons in pristine, glaciated mountain environments should address the extent to which pollutants in solution act like water molecules or whether they are more susceptible to, for example, refreezing into the surrounding ice, becoming stuck in micro-fractures and pore spaces, or sorption onto subglacial sediments.

HESSD

11, 13711–13744, 2014

1 Introduction

Dye tracing provides an opportunity to study the otherwise unseen drainage system inside and underneath glaciers. Measuring the rapidity and pattern of dye emergence, as well the quantity of dye recovered at the proglacial outlet, can provide important insight into the form and efficiency of the glacier drainage system. Dye tracing has been applied successfully in the alpine environment in several studies and has contributed substantially to understanding of subglacial drainage systems, for example, Storglaciären in the Kebnekaise mountains in northern Sweden (e.g. Seaberg et al., 1988; Hock and Hooke, 1993), glaciers in the European Alps (e.g. Nienow et al., 1998), the High Artic (e.g. Bingham et al., 2005) and, more recently, the Greenland Ice Sheet (Chandler et al., 2013; Cowton et al., 2013). More generally, the number of extensive dye tracer studies of glaciers is still limited (Willis et al., 2012), and basic unresolved issues remain in understanding the temporal and spatial variability of glacial drainage systems, the extent of efficient drainage, and the morphology of englacial and subglacial drainage.

The distribution of advective travel times derived from tracer experiments also provide an essential basis in quantifying large-scale transport and attenuation-retention processes that govern catchment-scale contaminant spreading (Darracq et al., 2010; Destouni et al., 2010). The here considered Rabots glaciär in Kebnekaise mountains was subject to a large spill of hydrocarbons, originating from a crash of a Royal Norwegian Air Force Lockheed Martin C-130J Super Hercules aircraft on 15 March 2012. The aircraft crashed into the western face of Kebnekaise, approximately 50 m below the mountain ridge, during a military exercise. Of the initial 14 100 L of kerosene jet fuel on board at take-off, an estimated minimum of 11 100 L was sprayed over the snow and ice-covered mountain environment, together with 50 L of hydraulic oil and 170 L of turbo oil (Rosqvist et al., 2014). Some of it was subsequently swept down and buried on Rabots glaciär by a large snow avalanche along with the wreckage. Wreckage debris was found on neighbouring Storglaciären and Björlings glacier, but the majority was

HESSD
11, 13711–13744, 2014

deposited on Rabots glaciär, which was not subject to immediate clean-up or decontamination of fuel due to the hazardous nature of the impact site and the large volume of snow affected.

Extensive plumes of dissolved contaminants often develop down-gradient of hydrocarbon source zones, as for instance shown through monitoring of numerous spills in industrial areas (e.g., Jarsjö et al., 2005). To understand potential adverse environmental impacts of the Kebnekaise accident, it is imperative to characterise the transport of dissolved constituents with glacial meltwater through Rabots glaciär. In addition, hydrocarbons that remain after volatilization (e.g., Jarsjö et al., 1994) may also move with water in free (non-dissolved) phase; for instance, relatively light hydrocarbon mixtures like kerosene will float on top of water-saturated zones (e.g., Schwille, 1981). Hydrocarbons were detected in the snow pack of the pollution source zone on Rabots glaciär (Fig. 1) and at sporadic intervals in the proglacial river system during the 2013 melt season (Rosqvist et al., 2014). This provides evidence for active advection of pollutants through the glacier system during 2013, the rapidity and transit pathways of which are discussed here following the application of dye tracing. The pathways for transport of hydrocarbon pollution through a full glacier system have never before been studied, and thus dye tracing is imperative if we are to understand anything about advective travel times of pollutants in a glacier system.

Here, we present the results of dye tracing experiments conducted as part of a monitoring programme on Rabots glaciär during the 2013 melt season, commissioned by the National Property Board of Sweden (Statens Fastighetsverk). The main objectives are: (i) to use dye breakthrough curve characteristics to determine pathways for transport of hydrocarbon pollution from the source zone to the proglacial environment, (ii) provide new temporal and spatial information on the previously little-studied hydrological system of Rabots glaciär, and (iii) obtain and interpret the discharge and turbidity of Rabots proglacial river system. Rabots glaciär has received relatively little attention compared to neighbouring Storglaciären, which is the best studied glacier in Sweden (e.g. Schytt, 1981; Holmlund, 1988; Jansson, 1996; Schneider, 1999; Glasser

HESSD
11, 13711–13744, 2014

et al., 2003), and an understanding of its hydrological system has been extremely limited until now. The majority of dye tracing experiments in moulins on Storglaciären have been conducted in the lower ablation zone (e.g. Seaberg et al., 1988; Hock and Hooke, 1993; Kohler, 1995); during fieldwork on Rabots glaciär moulins have been found distributed over a greater altitudinal range. Dye tracing experiments conducted in crevasses, moulins or boreholes at elevations above the riegel under Storglaciären have been limited and produced very attenuated, or, in some cases, no return of dye (Hooke et al., 1988; Jansson, 1996). The results presented below thus not only inform about pathways for the transport of hydrocarbon pollution, but also give new insight to the workings of the hydrology of Rabots glaciär and its similarities and contrasts with Storglaciären.

2 Site description

Rabots glaciär is a small, 3.1 km^2, polythermal valley glacier, situated on the western side of Kebnekaise (2099 m a.s.l.) in sub-Arctic Sweden (Fig. 1). The glacier extends from 1848 m a.s.l. at its highest point down to 1111 m a.s.l. at the snout, with an average slope of 11.5°. The maximum recorded Little Ice Age (LIA) extent of Rabots glaciär dates to 1910, as captured in photographs taken in 1910 by Enqvist (Brugger and Pankratz, 2014). In comparison to neighbouring Storglaciären, which has been characterised by a relatively stable terminus position in the last ca. 20 years, significant retreat of Rabots glaciär from its LIA maximum and thinning continues due to its longer response time to climatic changes (Brugger, 2007). Radio-echo sounding conducted in 1979 found that Rabots glaciär had a maximum ice thickness of 175 m, with an average of 84 m (Björnsson, 1981). It also revealed that the subglacial topography underneath Rabots glaciär is gently sloping with no pronounced overdeepenings. This is in strong comparison to Storglaciären, for which the bed is characterised by several subglacial overdeepenings and a pronounced bedrock riegel (Björnsson, 1981). One may then expect Rabots glaciär to exhibit different hydrological behaviour due to the

HESSD
11, 13711–13744, 2014

less complex nature of topography beneath the glacier. Meltwater at the terminus of Rabots glaciär leaves primarily through two proglacial streams. The high turbidity of the northernmost of these streams indicates that it has much more interaction with bed sediments than its relatively clear southern counterpart. The proglacial environment is characterized by several braided systems that travel through an overridden inner moraine and a pronounced terminal moraine (Karlén 1973). The overall hydrological catchment size amounts to 9 km^2 with an ice covered area of 33 %.

3 Method

3.1 Meteorological data

Meteorological data were recorded between April and September 2013 by an automatic weather station at 1355 m a.s.l. on Rabots glaciär. Meteorological variables, including air temperature and precipitation, were measured every minute and the mean of these measurements stored at 15 min intervals. Air temperature was measured at 0.5, 1 and 2 m above the surface using HygroClip T/Rh sensors and recorded as both transient and average values. Total precipitation was recorded by a Young unheated tipping bucket rain gauge.

3.2 Proglacial river discharge

River gauging was conducted at a stable bedrock location in the proglacial river during the 2013 melt season, ca. 1.5 km downstream of the glacier terminus. This location permitted convergence of the proglacial outlets and for measurement at an area of constrained flow downstream of the numerous braided systems operating between terminal moraines. Measurements of both river stage and of air and water pressure were conducted between days 181 and 249. Stage was measured by a SR50A sonic ranging sensor and pressure was recorded by HOBO U20 data loggers. Discharge time series were constructed from both relative gauging height (every 15 min) and relative

HESSD
11, 13711–13744, 2014

water pressure (every 10 min) based on a ratings curve produced by relating measured stage and pressure to discharge calculated for repeated rhodamine dye tracings (D1 to D5; Table 1) in the proglacial river.

3.3 Dye tracing

Field campaigns targeting glacial hydrology were conducted during July and August 2013, during which 17 dye tracing experiments were conducted to quantify transit times and pathways for meltwater flow through crevasses in the upper reaches of the glacier, moulins throughout the ablation zone (Fig. 2), and in the proglacial river (Table 1). A known quantity of Rhodamine water tracer 20 % solution (RWT) was used in the majority of dye tracer experiments, with Uranine (Na Fluorescein) 33.3 % solution used when simultaneous experiments were desired. Uranine is susceptible to photodegradation, so injection was conducted as close as safely possible to the englacial opening to reduce time exposed to sunlight. Dye was injected into flowing water in every case, upstream of open crevasses and moulins. Emergence of the dyes was measured using both manual sampling and automated detection methods, and for all experiments, the sampling rates for both automatic and manual detection were less than 1/16 of the residence time, suggested by Nienow et al. (1996) to be a maximum acceptable measurement period.

For automated detection of dye emergence, an Albillia GGUN-FL30 field fluorometer was stationed in the proglacial stream (Figs. 1 and 2), and was monitored at regular intervals to check the stability of the sonde within the stream. The FL30 is a flow-through fluorometer with a minimum detection limit of ca. 2×10^{-11} g mL^{-1}, and allows detection of 3 separate tracers simultaneously, in addition to measuring turbidity and water temperature, at a sampling rate up to 2 s. In order to establish the preferential flow pathway for meltwater originating at the hydrocarbon source zone, water samples were taken manually in both of the main streams emerging from the glacier front (Figs. 1 and 2) during experiment A7. The samples were analysed for fluorescence with a Turner Designs AquaFluor handheld fluorometer, set up for Rhodamine WT at a minimum

HESSD
11, 13711–13744, 2014

detection limit of 0.4 ppb. Based on calibration of the instruments (for a 100 ppb solution), fluorescence was converted to dye return concentration to produce breakthrough curves for each experiment. These dye returns were subsequently used to calculate the throughflow velocity, dispersion coefficient, dispersivity, storage retardation and dye recovery for each successful experiment (Table 2).

3.4 Dye breakthrough analysis

For each dye return a modelled concentration-time (breakthrough) curve was calculated using an advection-dispersion model (Brugman, 1986; Seaberg et al., 1988; Cowton et al., 2013), at a temporal resolution of 30 s. The concentration of dye is represented as c at time t, where V_0 represents the volume of injected dye, and Q is discharge ($m^3 s^{-1}$), which was allowed to vary freely in order to produce a best fit to the measured breakthrough curve for each experiment (Willis et al., 1990, 2009). Variation of Q was permitted even for the August experiments where Q was measured, since discharge does not remain constant throughout an experiment, and to account for error associated with deriving discharge from a ratings curve:

$$c(t) = \frac{v}{Q} \frac{V_0}{\sqrt{(4\pi D t)}} \exp - \frac{(x - vt)^2}{4Dt} \quad (1)$$

Throughflow velocity, or transit speed, v ($m s^{-1}$), for each experiment is calculated as:

$$v = \frac{x}{t_m} \quad (2)$$

where the transit distance x (m) is the straight line distance between the injection point and sampling location, and the residence time t_m (s) is the time between dye injection and peak concentration. This value was corrected for travel time in the stream during the August experiments to account for the different positioning of the FL30 fluorometer in July and August. The dispersion coefficient D ($m^2 s^{-1}$) in Eq. (1) indicates the rate

HESSD
11, 13711–13744, 2014

at which dye spreads within the glacier hydrological system (Willis et al., 2009). The variable t_j represents the time taken until half of the peak concentration on the rising ($t_j = t_1$) and falling limb ($t_j = t_2$) of the measured dye return curve. The equation is solved iteratively for t_m for both $t_j = t_1$ and $t_j = t_2$ until the equations converge to obtain the same value of D (Seaberg et al., 1988):

$$D = \frac{x^2(t_m - t_j)^2}{4t_m^2 t_j \ln\left(2\sqrt{\frac{t_m}{t_j}}\right)} \quad (3)$$

Dispersivity, d (m), is further calculated to describe the spreading rate of dye relative to the transit velocity through the glacier, providing an inference for transit route complexity (Seaberg et al., 1988; Willis et al., 1990):

$$d = \frac{D}{v} \quad (4)$$

Temporary storage of dye in the glacier results in elongation of the falling limb of the modelled return curve, and is not accounted for in the advection-dispersion model (Seaberg et al., 1988; Schuler et al., 2004). To examine this, storage retardation, SR, is thus quantified as the percentage area difference under the measured and modelled falling limbs (Nienow, 1993; Schuler, 2002; Cowton et al., 2013). The higher the SR, the lower the fit between the modelled and measured curve, thus the higher the temporary storage. Further, dye recovery, W (g), describes the weight of dye which passed through the fluorometer during an experiment, where dt is the logger interval in seconds, and Q is the average measured discharge for the duration of the experiment:

$$W = \sum_{t=1}^{n} cQ\mathrm{d}t \quad (5)$$

HESSD
11, 13711–13744, 2014

The percentage dye recovery can then be expressed as a percentage, W %, where W_0 is the initial mass of the injected tracer:

$$W\,\% = 100\frac{W}{W_0} \tag{6}$$

4 Results and discussion

4.1 Discharge

Discharge in the proglacial river remains relatively small throughout the measurement period, with an average of 1.79 $m^3 s^{-1}$. In response to relatively high temperatures in July (Fig. 3), discharge reaches a maximum of 3.92 $m^3 s^{-1}$ on day 212, before experiencing a step-wise decrease to a period of steady discharge averaging around ca. 1.3 $m^3 s^{-1}$ from day 221 to day 227. The second half of August is characterised by discharge fluctuating by ca. 2 $m^3 s^{-1}$ in response to rainfall events and periods of higher temperatures. Average discharge continues to fall into September. The diurnal cycle of discharge lags that of temperature, with peak discharge occurring daily on average ca. 2 h after peak recorded temperature, representing the response time of the river to ablation and transit of meltwater through the glacier. The amplitude of the diurnal discharge cycle decreases throughout the melt season (Fig. 3).

4.2 Turbidity

The turbidity of the proglacial river system, recorded in Nephelometric Turbidity Units (NTU), was not measured continuously throughout the season, but measured contemporaneously with dye fluorescence at the river gauging station (Fig. 2) during 6 out of 10 days in August 2013. Average peak discharge occurs within one hour of average peak turbidity (Fig. 4c), indicating that mobilisation of sediments leads discharge. Hysteresis is observed both at the diurnal scale and at a multi-day scale, over a period of 10 days

HESSD
11, 13711–13744, 2014

(Fig. 4a and b). Hysteresis is a behaviour for which a value of the dependent variable (turbidity) can vary for a given value of the independent variable (discharge) depending on whether the independent variable is increasing or decreasing (Hodgkins, 1996). At the diurnal scale hysteresis occurs only in a clockwise direction, while a figure-eight is produced at the multi-day scale, encompassing both clockwise and anticlockwise behaviour (Fig. 4a and b). Clockwise hysteresis infers that peak diurnal turbidity leads peak diurnal discharge, as exemplified in Fig. 4c, such that for equivalent discharge values on the rising and falling limbs of the hydrograph, turbidity is higher on the rising than the falling limb (Hodgkins, 1996). Clockwise hysteresis can be interpreted as easy mobilisation of fresh sediment flushed out from channel beds and margins, followed by an exhaustion of sediment supply (Hodgkins, 1996; Singh et al., 2005; Pietron et al., 2014). Given the short period of time over which turbidity was recorded at Rabots glaciär it is not possible to investigate multi-day evolution of sediment mobilisation over the melt season. However, within a limited period of 10 days we observe a figure-eight clockwise/anticlockwise hysteresis loop (Fig. 4b). Conversely to clockwise behaviour, anticlockwise hysteresis implies that the peak in diurnal discharge leads the peak in diurnal turbidity, indicating that sediments are not as easily mobilised.

Diurnal observations of hysteresis in the proglacial river of Rabots glaciär were entirely clockwise, and are therefore comparable with the largely clockwise hysteresis recorded by Singh et al. (2005) for Gangotri Glacier in the Himalayas. Data collection in the Gangotri study, however, extended over a full melt season, much longer than our 10 day, non-continuous measurement period. One may compare further with observations of hysteresis at Scott Turnerbreen in Svalbard (Hodgkins, 1996), for which a progressive change in hysteresis from clockwise to anticlockwise was observed during the melt season. Scott Turnerbreen is a "cold-based", non-temperate glacier (Hodgkins, 1996), while Rabots glaciär is polythermal, and because of differences in the glacier hydrological system, particularly at the bed, this may explain why we do not see anticlockwise diurnal hysteresis in the late melt season at Rabots glaciär. Temperate Bench glacier in Alaska has also been observed to produce clockwise behaviour, including

HESSD
11, 13711–13744, 2014

during two flood events (Riihimaki et al., 2005). The anticlockwise pattern observed between days 220 and 222 (Fig. 4b) follows a period of increased temperatures between days 217 to 219 (Fig. 3). Sediments within the glacier system may have been flushed out, and sourced from higher elevation, during this period due to higher melt rates, followed by a period of sediment exhaustion. This may have been exacerbated by the prevalence of silty sediments subject to strong cohesion in the glacier forefield, reducing the possibility for sediment mobilisation. The sharp increase in turbidity in the Rabots glaciär proglacial stream during day 228 is likely a reflection of a peak in temperature, lagged by a peak in discharge (Fig. 3). We hypothesise that increased temperature, and thus increased meltwater availability, combined with a precipitation event, may have permitted extension of the network of subglacial conduits during this period, allowing access to a fresh sediment supply at the glacier bed, as also observed by Riihimaki et al. (2005). Easy mobilisation of sediments at Rabots glaciär may be a source of pollution spreading and transport, where pollutants sorb to sediment particles.

4.3 Dye breakthrough

Results from calculation of analytical dye return parameters for each experiment are listed in Table 2, along with discharge calculated for each experiment based on measurements in the proglacial river. Measured breakthrough curves are illustrated for each successful glacier dye tracing experiment in Fig. 5. Modelled breakthrough curves and dye recovery are also depicted for the August experiments. Visual interpretations of the breakthrough curves reveal that there is a decrease in curve width with progression of the season, as well as an increase in symmetry. All curves except J1 and J2 exhibit a smooth asymmetric form, as observed elsewhere (e.g. Seaberg et al., 1988; Willis et al., 1990; Cowton et al., 2013), and are characterised by clear single peak return curves. Return curves J1 and J2 are more complex in form, with longer falling limbs that do not reach base level values before the end of the experiments. These curves are also characterised by a higher degree of noise, likely due to low dye recovery.

HESSD
11, 13711–13744, 2014

Experiment A7 was monitored simultaneously by both automated fluorescence detection and manual water sampling in both major proglacial outlets. The dye emerged only in the southernmost, less turbid proglacial outlet. The dye breakthrough curve derived from the analysis of water from manual sampling was in accordance with that from automated detection using the FL30 both in terms of form and emergence time. That manually-analysed breakthrough curve was, however, characterised by increased noise due to turbidity, which is not corrected for in manual sampling. The breakthrough curves of experiment A7 represent meltwater flow from as close to the source zone as was possible with the condition of flowing water for injection. Both curves reached their peak ca. 14 h after injection, after ca. 12 h with no dye signal. The residence time, form of the breakthrough curve, and emergence of the dye in only one (less turbid) proglacial outlet indicates temporary storage followed by an efficient release of meltwater, with little interaction with the bed substrate.

4.4 Throughflow velocities

Measured throughflow velocities are an average of flow velocities within the englacial and subglacial drainage system between the injection site and detection point. Throughflow velocities range from 0.04 to 0.28 $m\,s^{-1}$ for the glacier-based experiments (Table 2), which fall within the range of values previously inferred from experiments on Storglaciären (Seaberg et al., 1988; Hock and Hooke, 1993). A threshold of 0.2 $m\,s^{-1}$ is proposed by Theakstone and Knudsen (1981) and Nienow (2011) to distinguish between fast and slow flow. Willis et al. (2009) propose a similar threshold for fast flow, considering velocities of $< 0.05\,m\,s^{-1}$ as slow, $\sim 0.1\,m\,s^{-1}$ as moderate and $> 0.15\,m\,s^{-1}$ as fast. Flow velocities above the proposed thresholds for fast flow have traditionally been interpreted as indicative of channelised transport while flow velocities below the threshold indicate distributed water routing (Seaberg et al., 1988; Willis et al., 1990; Cowton et al., 2013). Throughflow velocities in the Rabots proglacial river reached a maximum of 0.58 $m\,s^{-1}$. We observe no clear relationship between velocity and elevation for experiments on the glacier, or between velocity and time into the sea-

HESSD
11, 13711–13744, 2014

son. The lowest values of throughflow velocity were calculated for experiment A7, and we hypothesise that they are representative of a relatively long period of initial storage before more rapid flow following a sudden meltwater release.

Following Leopold and Maddock (1954), the relationship between throughflow velocity and discharge can be expressed as a simple power function. There is a positive correlation between throughflow and discharge both for glacier-based dye returns ($R^2 = 0.65$) and proglacial returns ($R^2 = 0.27$) at Rabots glaciär (Fig. 6). The results of this study are compared against those from neighbouring polythermal Storglaciären (Seaberg et al., 1988) and temperate outlet glacier Midtdalsbreen, Norway (Willis et al., 1990) in Table 3. Seaberg et al. (1988) differentiated between proglacial and sub/englacial flow, while Willis et al. (1990) divided recorded discharge two tributary systems T1 and T3, which were interpreted as draining two different glacial hydrological systems. In the proglacial system of Rabots glaciär, velocity increases with the 0.6 power of the discharge. The associated multiplier is lower than that calculated for Sydjokk, one of the proglacial rivers of neighbouring Storglaciären (Seaberg et al., 1988), such that velocity through Sydjokk is 2.8 times larger than for the Rabots glaciär proglacial river. The braided nature of the Rabots proglacial river as it navigates through the proglacial outwash plain and terminal moraines may explain this difference.

The exponent of the en- and subglacial drainage is also significantly higher in this study compared with Storglaciären and Midtdalsbreen, while the multiplier is in the same order as that for Midtdalsbreen. For a given discharge, the velocity of water flowing en- or subglacially or both in Rabots glaciär is thus 2–3 times lower than Midtdalsbreen, and 13 times lower than Storglaciären. The much larger exponent for en/subglacial flow through Rabots glaciär may indicate that discharge is accommodated by an increase in hydraulic gradient within the system due to backing up of water, and by decreasing sinuosity, as proposed both for Storglaciären (Seaberg et al., 1988) and T1 of Midtdalsbreen (Willis et al., 1990), rather than through changes in cross-sectional channel area. Cowton et al. (2013) and Nienow et al. (1998) state that a flow in a channelised system is expected to be 1–2 orders of magnitude higher than

HESSD
11, 13711–13744, 2014

in a distributed system. We do not see this order of magnitude difference in our data (Table 2), or an increase in velocity over time, which is likely a product of early onset melt and development of the drainage system.

4.5 Dispersivity

Dispersivity is a measure of the extent to which dye spreads out relative to the speed at which it travels downstream with meltwater (Willis et al., 1990). Low dispersivities (< 5 m) are typically indicative of efficient water routing, and high values of dispersivity (> 20 m) have been associated with drainage of decreased efficiency, possibly due to distributed drainage system form (Nienow et al., 1998; Bingham et al., 2005; Willis et al., 2009). Water that is stored either supraglacially or englacially may also increase the rate of dispersivity (Fountain, 1993; Schuler et al., 2004); for example through buffering of meltwater flow in snow and firn layers, or storage in englacial fracture networks. From visual interpretation of the return curves (Fig. 5) the elongation of the falling limb in relation to the rising limb decreases with time into the melt season. This is supported by falling values of both dispersivity and the dispersion coefficient (Table 2), with the exception of experiment A7, for which dispersivity experiences a fourfold increase compared to experiment A4. A7 was the highest elevation at which dye was injected, which likely explains the increase in dispersivity despite being late in the melt season (Fig. 7b).

We interpret the decrease in dispersivity over time (Table 2) as an increase in drainage system efficiency, despite a general decrease in discharge and its diurnal cyclicity after peak discharge in late July (Fig. 3). Furthermore, we find no significant relationship between dispersivity and either velocity or elevation (Fig. 7), with R^2 values of 0.19 and 0.35 respectively; instead we propose that the relationship between velocity and dispersivity is indicative of four distinct meltwater flow regimes. The first regime encompasses J1 and J2, which are characterised by both high dispersivity and relatively high throughflow velocities despite occurring earliest in the field season, and are representative of lowest drainage system efficiency. The velocity values may imply

HESSD
11, 13711–13744, 2014

channelised but sinuous flow, possibly impeded by interaction with basal sediments down the relatively long flow pathways, resulting in noisy, multi-peaked breakthrough curves (Fig. 5). The second regime is represented by experiment J3, which depicts a large decrease in dispersivity, 17 days after experiment J2. The breakthrough curve in this case is single-peaked, but the elongated falling limb implies increased dispersivity, which may be explained through continued sediment interactions. The northernmost stream through which the July experiments likely exited the glacier is turbid, supporting extensive interaction with the bed sediments.

The third regime contains experiments A1, A2 and A4, which are the three lowest elevation experiments, characterised by low dispersivities and throughflow velocities in excess of 0.18 m s^{1}. Flow through these moulins has the shortest travel pathway through the system, aided by the largest increase in drainage system efficiency due to the low elevation and time into the melt season. Experiments A3 and A7 fall under flow regime four, characterised by low throughflow velocities, and relatively low dispersivity in comparison to the July experiments. The form of the breakthrough curves for A3 and A7 is single-peaked, which, in addition to the relatively low dispersivities, supports channelised flow, despite low throughflow velocities. Injection point A3 is located just upstream of the moulins used for experiments A1, A2 and A4 (flow regime three). Despite this, there is a considerably increase in residence time for experiment A3; at least 2.5 h longer than for flow regime three. The residence time of A7 is the longest of the successful experiments, at ca. 14 h, characterised by a broad yet single-peaked return curve (Fig. 5). We interpret the behaviour displayed by the return curve of experiment A7 as reflecting sub/englacial meltwater storage followed by periodic release through an efficient system. This explains the long residence time and the unrepresentatively low throughflow velocities. Experiments A5 and A6 (Figs. 1 and 2) did not produce a dye breakthrough, indicating residence times longer than our detection period during day 222 of ca.11 h. Temperature, precipitation and discharge were all relatively low during this period (Fig. 3), perhaps indicating refreezing in the glacial hydrological system at the relatively high elevation of ca. 1350 m a.s.l.

HESSD
11, 13711–13744, 2014

4.6 Meltwater storage and flow constraints

The temporary storage of dye can be viewed as an influencing factor on dispersion, which manifests itself as an elongation in the falling limb of modelled return curves (Fig. 5; Willis et al., 2009; Cowton et al., 2013). With the exception of experiment A7, results show a 60 % reduction in storage retardation from glacier-based tests over time (Table 2). The largest storage values correspond with the more complex breakthrough curves returned from the July experiments, relating to high dispersivity and a less efficient drainage system. As throughflow velocities showed no increase with time, we propose that the reduction in storage retardation over time relates to increasing efficiency, and decreasing sinuosity, rather than evolution from a true distributed system to a channelised system, which had likely already formed due to early onset of melt in 2013. Similar behaviour was reported by Cowton et al. (2013) for the Leverett Glacier, southwest Greenland. Low dye recovery was calculated for experiments A2 and A4. Uranine was used as a tracer in these experiments, thus low dye recovery is likely accounted for by photochemical decay of the dye between emergence from the glacier terminus and detection by the fluorometer downstream.

Combined with a very low dye recovery (Table 2), the mechanism of storage and release proposed to explain the return curve of experiment A7 may be indicative of storage in the englacial system (Fountain, 1993; Cowton et al., 2013). In this case, quantities of the injected dye, which become dilute as more meltwater enters the system, may be released periodically, resulting in a low dye recovery and a smooth, single-peaked, *efficient* breakthrough curve with an elongated falling limb. This hypothesis is strengthened by the 5 % storage retardation calculated for automated sampling during the experiment (Table 2). Sporadic detection of hydrocarbons in the proglacial system (Rosqvist et al., 2014), rather than continuous emergence of pollutants, further attests to periodic release of meltwater and pollutants stored within the en-/subglacial hydrological system. The stream in which dye emergence from experiment A7 was detected manually has a very low turbidity in comparison to its northern counterpart, which al-

HESSD
11, 13711–13744, 2014

lows us to further hypothesize that meltwater emerging in the southern proglacial outlet interacts with the bed to a lesser degree, and is possibly routed downstream for a long distance within the englacial system. Low recovery rates for both manual and automated sampling of experiment A7 may be exacerbated by refreezing of dye onto the ice since dye detection continued overnight, during falling temperatures and very low discharge. The surface structure of Rabots glaciär is characterised by three major flow units emerging from the accumulation zone (Fig. 8), which partition the tongue longitudinally and create structural independence between units (Jennings et al., 2014). Structural weaknesses and longitudinal foliation along the boundaries of these flow units may provide a pathway for englacial meltwater flow, in addition to supraglacial flow as described by Hambrey (1977). The presence of flow units may thus constrain the flow of meltwater and pollutants from the source zone to the south side of the glacier, emerging in the southernmost proglacial outlet, as observed for experiment A7.

With the exception of experiment D1, proglacial dye experiments for production of a ratings curve resulted in recovery of at least 78 % of the dye, with sorption to sediment particles likely to contribute to this result. Storage retardation varied between 18 and 38 %, and for three of these experiments storage retardation exceeded the percentage of dye that was not recovered. This overestimation of storage retardation may be attributed to the advection-dispersion model, which was adjusted to the best fit of the model efficiency criteria, and for which only the falling limb of the breakthrough curve is considered.

5 Conclusions and implications

The results of dye tracing experiments provide a new and unique insight to the internal hydrological system of Rabots glaciär, and offer an understanding of the pathways and transit times of pollutants through the glacier. In response to an early start to the melt season, development of efficient drainage began in July, with return curves supporting

HESSD
11, 13711–13744, 2014

increased efficiency and decreasing sinuosity throughout August. Analysis of proglacial discharge and turbidity attests further to formation of efficient subglacial drainage, with clockwise hysteresis supporting easy mobilisation of sediments readily available within channels, thus also any pollutants that may have sorbed onto sediments. More extensive dye tracing studies are necessary to explore the full seasonal evolution of the Rabots glaciär hydrological system. Nevertheless, this study provides a first insight to the drainage system topology, and hints towards a possible structural control on meltwater flow pathways, which should be explored further in future studies in concert with an investigation of the internal thermal structure of the glacier. Although limited in number, the results of these experiments suggest that in comparison to Storglaciären, the internal hydrological system of Rabots is characterised by a degree of homogeny over a larger altitudinal extent, although constrained and divided laterally by the ice flow and structure of the glacier.

Assuming flow of pollutants in solution *with* meltwater, the delayed but efficient form of breakthrough curve A7, combined with a very low percentage dye return, may indicate that pollutants are being periodically released from an en-/subglacial store after entering the internal glacier hydrological system near the source zone. This is supported by sporadic rather than continuous detection of hydrocarbons in the proglacial river system. Experiment A7, from directly downstream of the source zone, estimates a transit time of ca. 15 h for transport through the full en-/subglacial hydrological system. This is likely an upper estimate for transit time as the hydrological system is well-developed by mid-August, producing efficient breakthrough of dye, even for experiment A7 which originated above 1350 m a.s.l. and a very short distance from the remaining snowpack. Snow is highly permeable and thus unlikely to retain pollutants at the multi-year scale, so we may expect to see storage of pollutants in the firn layer and ice mass, through percolation or firnification, subsequently released gradually by melt processes during melt seasons. Storage within firn and ice, or within the internal hydrological system, provides an opportunity for refreezing, further increasing the permanence of pollutants in the glacier system. Additional study is thus necessary to determine

HESSD
11, 13711–13744, 2014

the extent to which pollutants in solution act like water molecules or whether they are more susceptible to, for example, refreezing into the surrounding ice, becoming stuck in micro-fractures and pore spaces, or sorption onto subglacial sediments.

This research offers a unique insight to the transport pathways for pollutants through a full glacier system, contributing towards a broader analysis of the spread and longevity of hydrocarbon pollutants in the Rabots glaciär catchment. With increasing pressure on locations such as Kebnekaise from anthropogenic activity, and the environmental risks associated with these activities, our work provides a basis from which to create a new knowledge base for the analysis and action required following hydrocarbon spills in the glaciated Arctic mountain environment.

Author contributions. C. C. Clason led and all other authors contributed to the writing of the manuscript. Fieldwork was conducted by all authors, C. C. Clason designed the glacier hydrological experiments, C. Coch and C. C. Clason analysed the data and prepared figures.

Acknowledgements. This work was funded in 2012 by Formas (grant number BR9912A to G. Rosqvist) and Statens Fastighetsverk. We wish to thank Torbjörn Karlin, Susanne Ingvander, Ane LaBianca, Andrew Mercer, Pia Eriksson and Victor Plevrakis for their help in instrumentation set-up and data collection in the field, and Per Holmlund for providing imagery. We also wish to thank Christian Helanow for helpful discussion that improved the manuscript. K. Brugger gratefully acknowledges financial support from the University of Minnesota, Morris' Faculty Research Enhancement Funds.

References

Bingham, R. G., Nienow, P., Sharp, M. J., and Boon, S.: Subglacial drainage processes at a High Arctic polythermal valley glacier, J. Glaciol., 51, 15–24, doi:10.3189/172756505781829520, 2005.

Bjornsson, H.: Radio-echo sounding maps of Storglaciären, Isfallsglaciären and Rabots glaciär, northern Sweden, Geogr. Ann. A, 63, 225–231, 1981.

HESSD
11, 13711–13744, 2014

Brugger, K. A.: The non-synchronous response of Rabots Glaciär and Storglaciären, northern Sweden, to recent climate change: a comparative study, Ann. Glaciol., 46, 275–282, doi:10.3189/172756407782871369, 2007.
Brugger, K. A. and Pankratz, L.: Changes in the geometry and volume of Rabots glaciär, Sweden, 2003–2011: recent accelerated volume loss linked to more negative summer balances, Geogr. Ann. A, doi:10.1111/geoa.12062, online first, 2014.
Brugman, M. M.: Water flow at the base of a surging glacier, Ph.D. thesis, California Institute of Technology, unpublished, 1986.
Chandler, D. M., Wadham, J. L., Lis, G. P., Cowton, T., Sole, A., Bartholomew, I., Telling, J., Nienow, P., Bagshaw, E. B., Mair, D., Vinen, S., and Hubbard, A.: Evolution of the subglacial drainage system beneath the Greenland Ice Sheet revealed by tracers, Nat. Geosci., 6, 195–198, 2013.
Cowton, T., Nienow, P., Sole, A., Wadham, J., Lis, G., Bartholomew, I., Mair, D., and Chandler, D.: Evolution of drainage system morphology at a land-terminating Greenlandic outlet glacier, J. Geophys. Res., 118, 1–13, doi:10.1029/2012JF002540, 2013.
Darracq, A., Destouni, G., Persson, K., Prieto, C., and Jarsjö, J.: Quantification of advective solute travel times and mass transport through hydrological catchments, Environ. Fluid Mech., 10, 103–120, 2010.
Destouni, G., Persson, K., Prieto, C., and Jarsjö, J.: General quantification of catchment-scale nutrient and pollutant transport through the subsurface to surface and coastal waters, Environ. Sci. Technol., 44, 2048–2055, 2010.
Fountain, A. G.: Geometry and flow conditions of subglacial water at South cascade glacier, Washington state, USA; an analysis of tracer injections, J. Glaciol., 30, 180–187, 1993.
Glasser, N. F., Hambrey, M. J., Etienne, J. L., Jansson, P., and Pettersson, R.: The origin and significance of debris-charged ridges at the surface of Storglaciären, northern Sweden, Geogr. Ann. A, 85, 127–147, 2003.
Hambrey, M. J.: Supraglacial drainage and its relationship to structure, with particular reference to Charles Rabots Bre, Okstindan, Norway, Norsk Geogr. Tidsskr., 31, 69–77, 1977.
Hock, R. and Hooke, R. L.: Evolution of the internal drainage system in the lower part of the ablation area of Storglaciären, Sweden, Geol. Soc. Am. Bull., 105, 537–546, doi:10.1130/0016-7606(1993)105<0537:EOTIDS>2.3.CO;2, 1993.
Hodgkins, R.: Seasonal trend in suspended-sediment transport from an Arctic glacier, and implications for drainage-system structure, Ann. Glaciol., 22, 147–151, 1996.

HESSD
11, 13711–13744, 2014

Holmlund, P.: Internal geometry and evolution of moulins, Storglaciären, Sweden, J. Glaciol., 34, 242–248, 1988.
Hooke, R. Le, B., Miller, S. B., and Kohler, J.: Character of the englacial and subglacial drainage system in the upper part of the ablation area of Storglaciaren, Sweden, J. Glaciol., 34, 228–231, 1988.
Jansson, P.: Dynamics and hydrology of a small polythermal valley glacier, Geogr. Ann. A, 78, 171–180, 1996.
Jarsjö, J., Destouni, G., and Yaron, B.: Retention and volatilisation of kerosene: laboratory experiments on glacial and post glacial soils, J. Contam. Hydrol., 17, 167–185, 1994.
Jarsjö, J., Bayer-Raich, M., and Ptak, T.: Monitoring groundwater contamination and delineating source zones at industrial sites: uncertainty analyses using integral pumping tests, J. Contam. Hydrol., 79, 107–134, 2005.
Jennings, S. J. A., Hambrey, M. J., and Glasser, N. F.: Ice flow-unit influence on glacier structure, debris entrainment and transport, Earth Surf. Proc. Land., 39, 1279–1292, 2014.
Karlén, W.: Holocene glacier and climatic variations, Kebnekaise mountains, Swedish Lapland, Geogr. Ann. A, 55, 29–63, 1973.
Kohler, J.: Determining the extent of pressurized flow beneath Storglaciären, Sweden, using results of tracer experiments and measurements of input and output discharge, J. Glaciol., 41, 217–231, 1995.
Leopold, L. B. and Maddock, T. J.: The hydraulic geometry of stream channels and some physiographic implications, U.S. Geological Survey Professional Paper, United States Government Printing Office, Washington DC, 252 pp., 1954.
Nienow, P. W.: Dye tracer investigations of glacier hydrological systems, Ph.D. thesis, Cambridge University, UK, 1993.
Nienow, P. W., Sharp, M., and Willis, I. C.: Sampling-rate effects on the properties of dye breakthrough curves from glaciers, J. Glaciol., 42, 184–189, 1996.
Nienow, P., Sharp, M., and Willis, I.: Seasonal changes in the morphology of the subglacial drainage system, Haut Glacier d'Arolla, Switzerland, Earth Surf. Proc. Land., 23, 825–843, doi:10.1002/(SICI)1096-9837(199809)23:9<825::AID-ESP893>3.0.CO;2-2, 1998.
Pietroń, J., Jarsjö, J., Romanchenko, A. O., and Chalov, S. R.: Model analyses of the contribution of in-channel processes to sediment concentration hysteresis loops, J. Hydrol., in review, 2014.

HESSD
11, 13711–13744, 2014

Riihimaki, C. A., MacGregor, K. R., Anderson, R. S., Anderson, S. P., and Loso, M. G.: Sediment evacuation and glacial erosion rates at a small alpine glacier, J. Geophys. Res., 110, F03003, doi:10.1029/2004JF000189, 2005.
Rosqvist, G., Jarsjö, J., and Clason, C.: Redovisning av 2013 års övervakning av utveckling och spridning av flygbränsle och oljeföroreningar i Kebnekaise efter Herculesolyckan 15 mars 2012, Tarfala Research Station report, 26 pp., 2014.
Schneider, T.: Water movement in the firn of Storglaciären, Sweden, J. Glaciol., 45, 286–294, doi:10.3189/002214399793377211, 1999.
Schuler, T.: Investigation of water drainage through an alpine glacier by tracer experiments and numerical modelling, Ph.D. thesis, Swiss Federal Institute of Technology, Zürich, Switzerland, 2002.
Schuler, T., Fischer, U. H., and Gudmundsson, G. H.: Diurnal variability of subglacial drainage conditions as revealed by tracer experiments, J. Geophys. Res., 109, F02008, doi:10.1029/2003JF000082, 2004.
Schwille, F.: Groundwater pollution in porous-media by fluids immiscible with water, Sci. Total Environ., 21, 173–185, 1981.
Schytt, V.: The net mass balance of Storglaciaren, Kebnekaise, Sweden, related to the height of the equilibrium line and to the height of the 500 mb surface, Geogr. Ann. A, 63, 219–223, 1981.
Seaberg, S. Z., Seaberg, J. Z., Hooke, R. Le, B., and Wiberg, D. W.: Character of the englacial and subglacial drainage system in the lower part of the ablation area of Storglaciären, Sweden, as revealed by dye-trace studies, J. Glaciol., 34, 217–227, 1988.
Singh, P., Haritashya, U. K., Ramasastri, K. S., and Kumar, N.: Diurnal variations in discharge and suspended sediment concentration, including runoff-delaying characteristics, of the Gangotri Glacier in the Garhwal Himalayas, Hydrol. Process., 19, 1445–1457, 2005.
Willis, I. C., Sharp, M. J., and Richards, K. S.: Configuration of the drainage system of Midtdalsbreen, Norway, as indicated by dye-tracing experiments, J. Glaciol., 36, 89–101, 1990.
Willis, I. C., Lawson, W., Owens, I., Jacobel, B., and Autridge, J.: Subglacial drainage system structure and morphology of Brewster Glacier, New Zealand, Hydrol. Process., 23, 384–396, doi:10.1002/hyp.7146, 2009.
Willis, I. C., Fitzsimmons, C. D., Melvold, K., Andreassen, L. M., and Giesen, R. H.: Structure, morphology and water flux of a subglacial drainage system, Midtdalsbreen, Norway, Hydrol. Process., 26, 3810–3829, doi:10.1002/hyp.8431, 2010.

HESSD
11, 13711–13744, 2014

Table 1. Dye tracing experiments conducted on Rabots glaciär and in the proglacial river during 2013. J denotes July, A denotes August and D represents proglacial experiments.

Code	Day of year, injection time (LT)	Injection site	Tracer	Amount (mL)	Sampling (rate in min)	Dye return
J1	185, 14:47	Supraglacial stream	RWT	125	Auto (0.03); Manual (10)	Yes
J2	186, 11:37	Crevasse	RWT	245	Auto (0.03); Manual (10)	Yes
J3	203, 12:00	Moulin	RWT	250	Auto (0.03); Manual (10)	Yes
A1	220, 16:33	Moulin	RWT	150	Auto (0.5)	Yes
A2	220, 16:46	Moulin	Uranine	100	Auto (0.5)	Yes
A3	221, 14:27	Moulin	RWT	150	Auto (0.5)	Yes
A4	221, 15:26	Moulin	Uranine	100	Auto (0.5)	Yes
A5	222, 13:33	Crevasse	Uranine	200	Auto (0.5)	No
A6	222, 15:10	Supraglacial stream	RWT	125	Auto (0.5)	No
A7	227, 13:16	Supraglacial stream	RWT	500	Auto (0.5); Manual (10)	Yes
D1	220, 12:40	River	RWT	30	Auto (0.5)	Yes
D2	222, 10:49	River	RWT	30	Auto (0.5)	Yes
D3	227, 12:37	River	RWT	60	Auto (0.5)	Yes
D4	230, 12:22	River	RWT	50	Auto (0.5)	Yes
D5	230, 13:26	River	RWT	100	Auto (0.5)	Yes

HESSD
11, 13711–13744, 2014

Table 2. Results of dye tracing analysis from automatic sampling of fluorescence (A7* is based on manual sampling in the southernmost proglacial outlet). Here, discharge for A and J experiments is that calculated from stage recorded at the river gauging station averaged over the duration of each experiment, and for D experiments is the computed discharge based on dye tracing for production of the ratings curve.

Code	Day of year, injection time (LT)	Transit distance (m)	Throughflow velocity ($m s^{-1}$)	Dispersion coefficient ($m^2 s^{-1}$)	Dispersivity (m)	Storage retardation (%)	Dye recovery (%)	Discharge ($m^3 s^{-1}$)
J1	185, 14:47	1469	0.28	24.27	86.24	70.82	n/a	n/a
J2	186, 11:37	2022	0.21	19.33	92.63	58.51	n/a	n/a
J3	203, 12:00	1165	0.15	4.04	27.79	43.86	n/a	n/a
A1	220, 16:33	655	0.25	2.84	11.59	10.71	70.70	2.01
A2	220, 16:46	703	0.19	0.81	4.25	13.84	18.79	2.00
A3	221, 14:27	829	0.06	0.19	2.89	10.78	78.69	1.61
A4	221, 15:26	488	0.23	1.22	5.34	11.03	8.77	1.60
A7	227, 13:16	2339	0.04	0.79	18.01	5.03	8.25	1.28
A7*	227, 13:16	2182	0.04	1.10	28.78	58.56	23.70	1.28
D1	220, 12:40	685	0.38	0.59	1.56	38.5	55.05	1.73
D2	222, 10:49	874	0.23	1.46	6.43	20.64	81.50	1.08
D3	227, 12:37	1237	0.36	2.91	8.11	24.77	93.52	1.28
D4	230, 12:22	408	0.24	0.10	0.41	17.80	77.69	2.36
D5	230, 13:26	1534	0.58	4.11	7.08	31.31	89.18	2.20

HESSD
11, 13711–13744, 2014

Table 3. Velocity-discharge analyses from Rabots glaciär, Sweden (this study), Storglaciären, Sweden (Seaberg et al., 1988) and Midtdalsbreen, Norway (Willis et al., 1990). Note that experiments were conducted over a period of two years for both Storglaciären and Midtdalsbreen.

Study	Domain	Sample size	Multiplier	Exponent	R^2
Clason et al. (this study)	proglacial	5	0.25	0.60	0.27
Clason et al. (this study)	sub/englacial	5	0.02	3.44	0.65
Seaberg et al. (1988)	proglacial	13	0.69	0.27	n. a.
Seaberg et al. (1988)	subglacial (Sydjokk)	6	0.26	1.00	n. a.
Willis et al. (1990)	sub/englacial (T1)	5	0.06	1.00	0.44
Willis et al. (1990)	sub/englacial (T3)	8	0.04	0.60	0.10

HESSD
11, 13711–13744, 2014

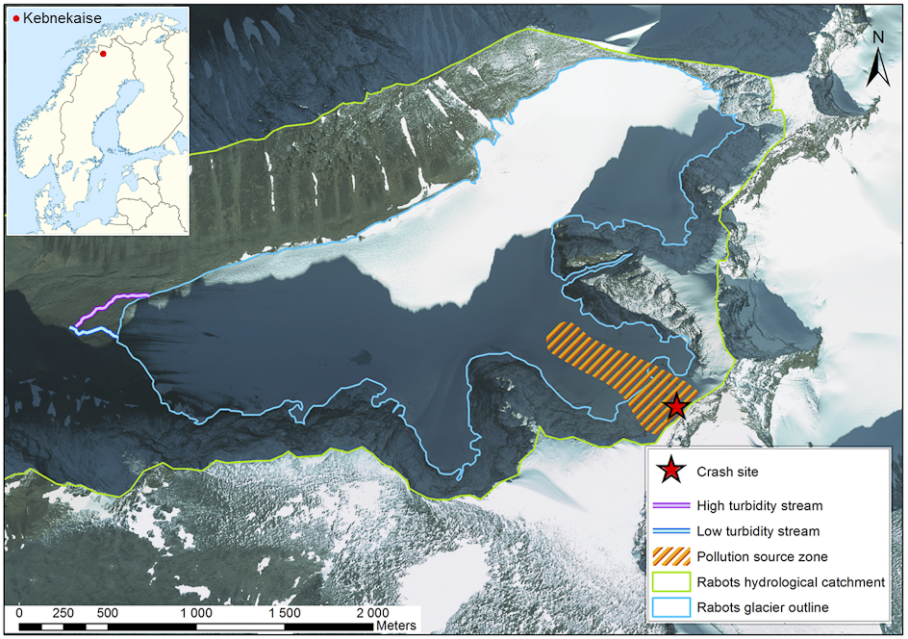

Figure 1. Rabots glaciär with glacier extent marked in blue and the hydrological catchment in green. The site of the plane impact is depicted by the red star, and the orange spotted area represents the estimated area of the initial source zone of hydrocarbon pollutants. The background image is an orthophoto captured in 2008 by Lantmäteriet.

HESSD
11, 13711–13744, 2014

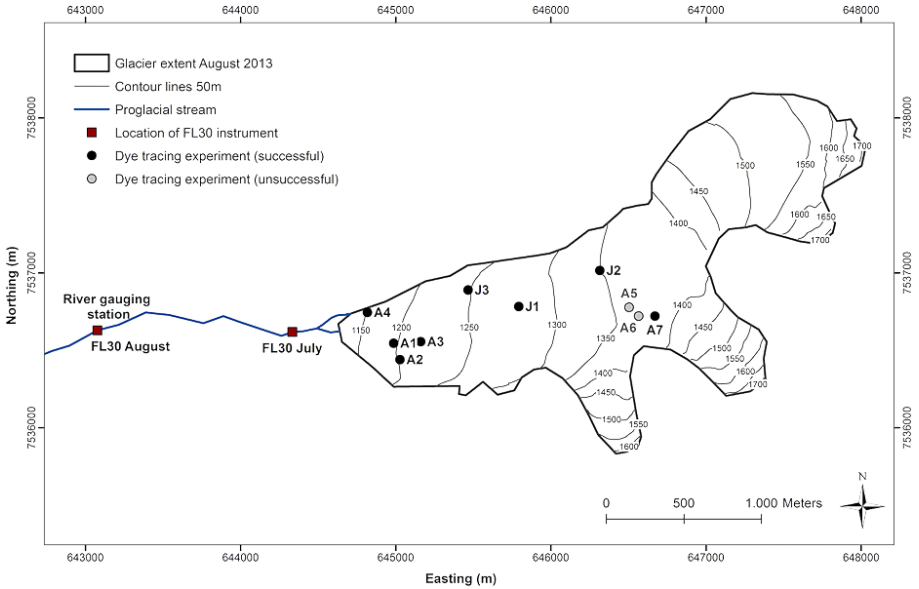

Figure 2. Locations of glacier-based dye tracing experiments during 2013.

HESSD
11, 13711–13744, 2014

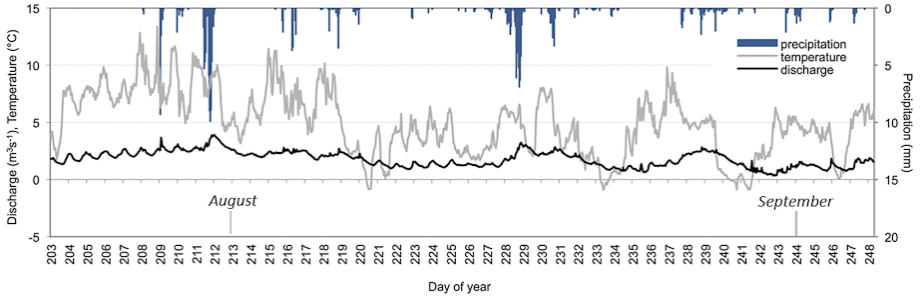

Figure 3. Measured 2 m temperature, precipitation and calculated discharge during summer 2013 (days span 22 July–5 September).

HESSD
11, 13711–13744, 2014

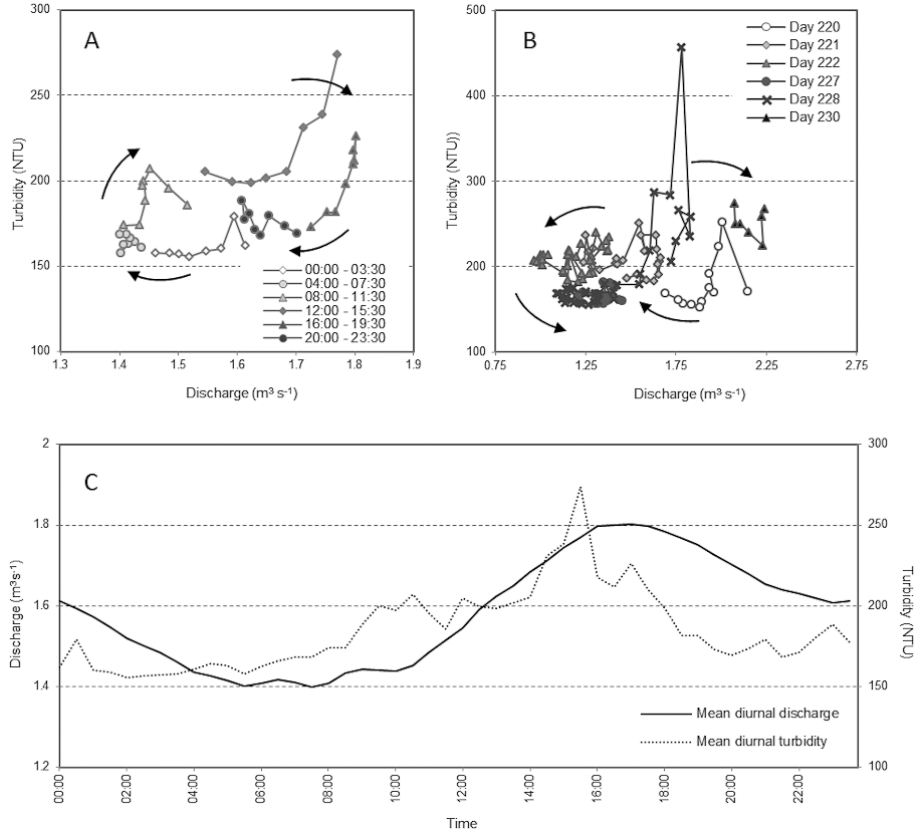

Figure 4. (a) Diurnal turbidity, averaged at 30 min intervals across all measurement days, plotted against mean diurnal discharge, **(b)** all available measurements of turbidity (30 min intervals) plotted against discharge, and **(c)** diurnal cycle of discharge and turbidity averaged at 30 min intervals for all available measurements between days 220 and 230.

HESSD
11, 13711–13744, 2014

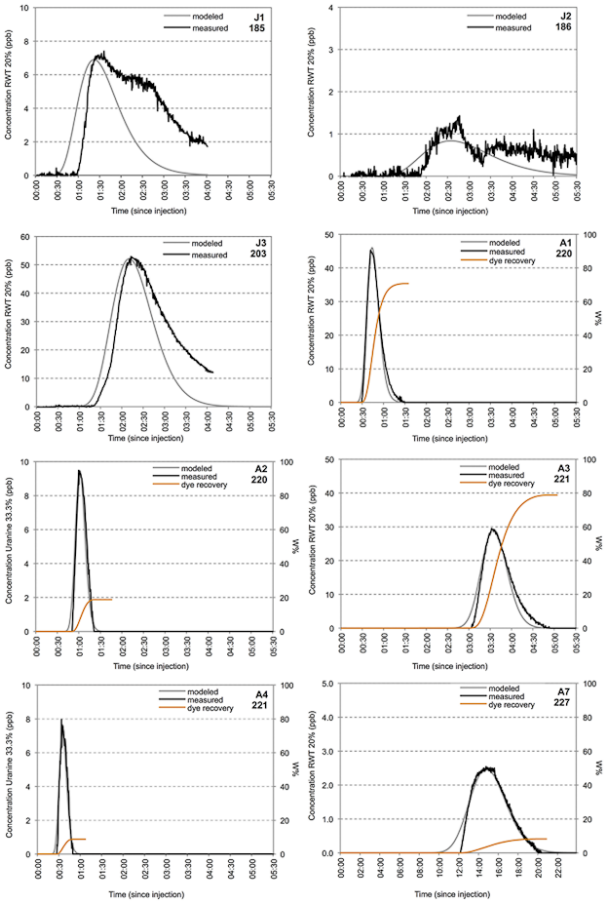

Figure 5. Modelled and measured dye breakthrough curves, including dye recovery for the August experiments. Note that the *x* axis for experiment A7 differs from the others due to the particularly long dye return time.

HESSD
11, 13711–13744, 2014

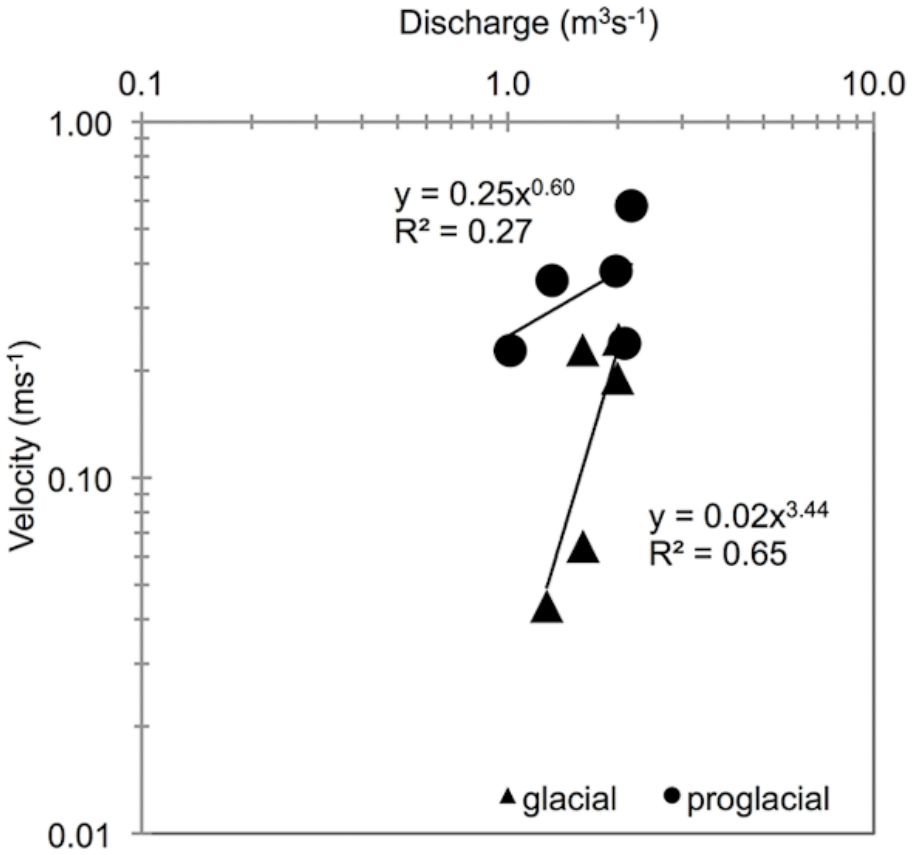

Figure 6. Velocity plotted against discharge for proglacial and glacier-based dye tests conducted during August 2013. Note that the July experiments are not included because there are no contemporaneous measurements of stage from which to calculate discharge.

HESSD
11, 13711–13744, 2014

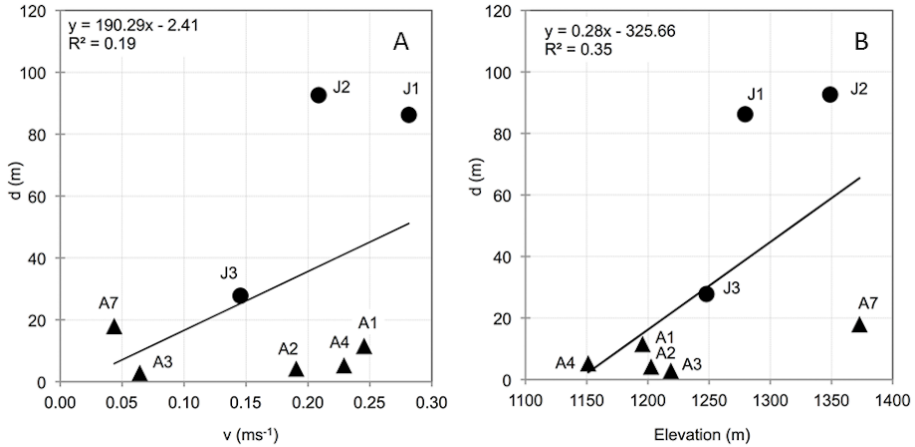

Figure 7. Variation of dispersivity relative to throughflow velocities **(a)** and elevation **(b)**.

HESSD
11, 13711–13744, 2014

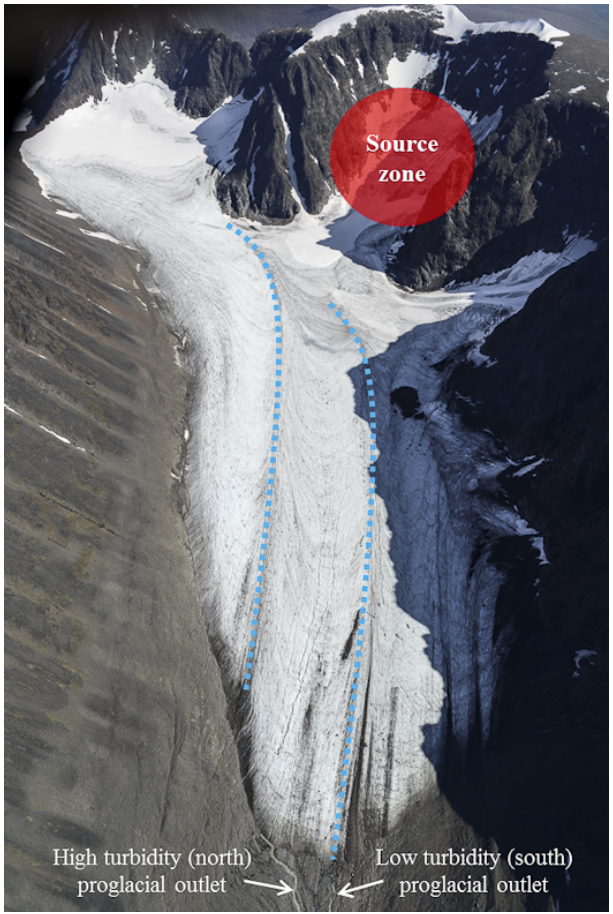

Figure 8. Surface structure of Rabots glaciär as seen from aerial photography taken on 9 August 2013. Blue dashed lines represent the boundaries between major flow units (photo credit: Per Holmlund).

HESSD
11, 13711–13744, 2014